

Three-dimensional modeling of magneto-optical trapping of MgF molecules with multilevel rate equations

Supeng Xu,¹ Meng Xia,¹ Ruoxi Gu,¹ Yanning Yin,¹ Liang Xu,¹ Yong Xia,^{1,2,*} and Jianping Yin¹

¹State Key Laboratory of Precision Spectroscopy, School of Physics and Materials Science, East China Normal University, Shanghai 200062, China

²NYU-ECNU Institute of Physics at NYU Shanghai, Shanghai 200062, China



(Received 1 August 2018; published 8 March 2019)

We present a theoretical study of magneto-optical trapping (MOT) force exerted on magnesium monofluoride (MgF) with three-dimensional rate equations, in which we have considered the complex vibrational and rotational levels and the effects of small internal splittings and degeneracies, including fine and hyperfine structures and the magnetic quantum numbers. We investigate the feasibility of MOT for MgF with a very small excited-state g factor ($g_e = -0.0002$) and a large radiative decay rate ($\Gamma = 2\pi \times 22$ MHz) for the electronic transition of $X^2\Sigma^+$ to $A^2\Pi_{1/2}$ states. We also optimize the MOT with reference to the three-, four-, and more-frequency component models with various polarization configurations and detunings. By applying the dual-frequency arrangement to more than one hyperfine level, we suggest a configuration of the (3 + 1)-frequency components for achieving the MOT of MgF.

DOI: [10.1103/PhysRevA.99.033408](https://doi.org/10.1103/PhysRevA.99.033408)

I. INTRODUCTION

The development of a molecular magneto-optical trapping (MOT) should really mirror the huge historical success achieved by the atomic MOT [1]. The realization of such a powerful technique for producing a diverse set of dense, ultracold diatomic molecular species opens a new chapter for molecular science and it will greatly advance understandings in precision measurement, complex quantum systems under precise control, and ultracold chemistry in the most fundamental way [2–4]. The dawn of ultracold polar molecules was signaled with the production of ground-state polar molecules KRb near quantum degeneracy in 2008 [5]. In that experiment, they bypassed the problem of direct cooling of molecules, taking advantage of ultracold atoms and then using resonant association techniques for producing ground-state molecules. This approach is currently limited to alkalis; such several recently created ultracold polar molecules also include RbCs [6,7], NaK [8], and NaRb [9]. On the other hand, tremendous progress has been made in direct laser cooling and the MOT of diatomic molecules, i.e., SrF [10,11], YO [12], CaF [13,14], triatomic molecule SrOH [15], and even polyatomic molecule CH₃F [16] and H₂CO [17]. In addition, some other ongoing candidates, such as YbF [18], BaF [19,20], and BaH [21], have attracted great interest as well. To date, the temperature of the cooled diatomic molecule is well below the Doppler limit [13,22,23]. The maximum number of molecules, 1.0×10^5 , were captured by Anderegg *et al.* through radio-frequency CaF MOT [14].

Magnesium monofluoride, due to its highly diagonal Franck-Condon factors and strong spontaneous radiation

decay, can also be a good candidate for molecular MOT [24]. In general, the magneto-optical trapping force is very weak if the excited-state g factor of the laser-cooling molecule, g_e , is much smaller than the ground-state g factor, g_g . Fortunately, due to the “dual-frequency effect” (the sublevel involved in the transition is addressed by two frequency components with different polarization at the same time, which is an effective way to eliminate the effect of the dark states) caused by the multiple levels in the ground state of the molecule, molecular force is no longer negligible compared to the atomic one [25]. However, note that MgF has a much smaller excited-state g_e ($g_e \approx -0.0002$), compared with CaF ($g_e \approx -0.021$) and SrF ($g_e \approx -0.088$) [26,27]. Also, note the unique hyperfine structure of the ground state [24] (the hyperfine level interval between the upper $F = 2$ and $F = 1$ levels of the ground state is $\sim 0.4\Gamma$, which may break down the dual frequency). So, it is necessary for us to verify whether or not MgF is appropriate for MOT and select the optimal polarization configuration.

In this paper, we apply three-dimensional (3D) multilevel rate equations with multiple frequencies of laser to model the MOT of the MgF molecule for the $A^2\Pi_{1/2} - X^2\Sigma^+$ transition. The dual-frequency mechanism is considered and we focus mainly on the choice of laser polarization and detuning. Throughout the discussion, we do not take the vibrational repump transitions into consideration since the influence on the MOT is small. Our results show that the three-frequency component can cool the molecule to a lower temperature, while the four-frequency component is preferred in trapping molecules. Moreover, by adding one extra frequency component, both the maximum damping force and the relatively large trapping force can be obtained at a cost of the capture velocity. These results will be an effective guide for our experiment.

*yxia@phy.ecnu.edu.cn

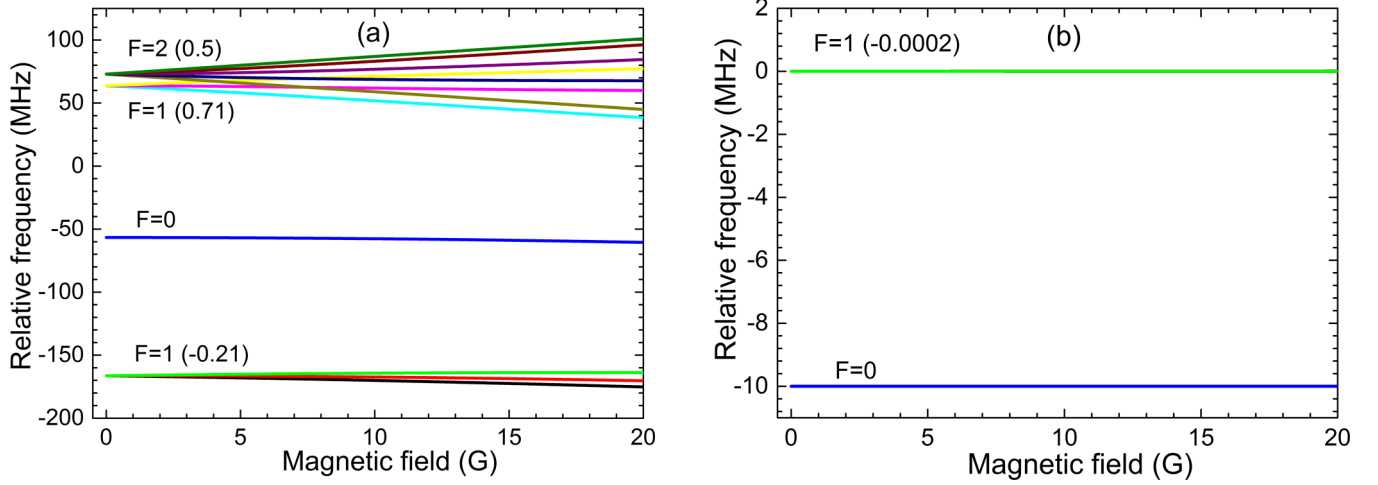


FIG. 1. Zeeman shifts of the states in magneto-optical trapping of MgF. (a) The four hyperfine components of the $X\ ^2\Sigma^+$ ($v=0$, $N=1$) state. (b) The two hyperfine components of the $A\ ^2\Pi_{1/2}$ ($v=0$, $J=1/2$) state with positive parity (e parity).

II. MODELING MOT OF MGF MOLECULE

A. Rate equations

We apply the approach of multilevel rate equations which include the dual-frequency effect to model the MOT of the MgF molecule [25,28]. The molecule has a set of ground states, g , and excited states, e , with populations n_g and n_e , respectively, interacting with a laser field with components p . Each laser component has an angular frequency ω_p and propagates in the direction of the unit vector κ_p . The frequencies are similar, so we use a single wavelength $\lambda \approx 2\pi c/\omega_p = 359.3$ nm for all components [29]. There is a quadrupole magnetic field represented by $B = A(x\hat{x}, y\hat{y}, -2z\hat{z})$, where \hat{x} , \hat{y} , \hat{z} are unit vectors in the x , y , and z axes, and A is the field gradient in the xy plane. According to our modeling, the magnetic field gradient will mainly influence the position of the peak, so we set $A = 30$ G/cm and $A = 10$ G/cm for the three- and four-frequency configurations, respectively. This ensures the minimum value of the trapping force within the beam-waist radius.

The intensity distribution of each laser beam is Gaussian,

$$I = \frac{2P}{\pi w^2} \exp\left(-\frac{2r^2}{w^2}\right) (r \leq r_t), \quad (1)$$

where r is the distance from the center of the beam, w is the $1/e^2$ radius, and P is the power of the beam. Taking into account the experimental feasibility, w is set to 12 mm in the following discussion.

All excited states share one decay rate Γ . The polarization of the laser is resolved into components (σ^- , π , σ^+) in the molecule's local coordinates, with relative amplitudes $(\frac{1}{2}, \frac{1}{\sqrt{2}}, \frac{1}{2})$, where the z axis is determined by the magnetic field direction. The molecules move slowly enough so they adiabatically follow the changes in the field direction. The rate equations for the system are

$$\dot{\mathbf{r}} = \mathbf{v}, \quad (2a)$$

$$\dot{\mathbf{v}} = \frac{h}{m\lambda} \sum_{e,g,p} \mathbf{k}_p R_{e,g,p} (n_g - n_e), \quad (2b)$$

$$\dot{n}_g = \Gamma \sum_e f_{e,g} n_e - \sum_{e,p} R_{e,g,p} (n_g - n_e), \quad (2c)$$

$$\dot{n}_e = -\Gamma n_e + \sum_{g,p} R_{e,g,p} (n_g - n_e), \quad (2d)$$

$$\dot{\gamma} = \Gamma \sum_e n_e. \quad (2f)$$

Here, m is the mass of the molecule, and \mathbf{r} and \mathbf{v} are the position and velocity of the molecule, respectively. Γ is the decay rate, γ is the number of scattered photons, $f_{e,g}$ is the branching ratio for spontaneous decay for the excited-state to ground-state (eg) transition, and $R_{e,g,p}$ is the excitation rate between levels e and g driven by laser component p , which is

$$R_{e,g,p} = \frac{\Gamma}{2} \frac{q_{e,g,p} s_p}{1 + 4(\delta_{e,g,p} - 2\pi \mathbf{k}_p \cdot \mathbf{v}/\lambda - \Delta\omega_{e,g})^2/\Gamma^2}, \quad (3)$$

where s_p is the saturation parameter, $q_{e,g,p}$ is the fractional strength of the transition being driven, $\delta_{e,g,p} = \omega_p - \omega_{e,g}$ is the detuning from the resonance angular frequency for a stationary particle at zero field, and $\Delta\omega_{e,g}$ is the Zeeman shift of the transition. For small magnetic fields, $\Delta\omega_{e,g} = (g_e M_e - g_g M_g) \mu_B B / \hbar$, where g_e , g_g are the g factors and M_e , M_g are the magnetic quantum numbers of the excited and ground levels, respectively. The saturation parameter is $s_p = I_p/I_{\text{sat}}$, where I_p is the intensity of laser component p , and $I_{\text{sat}} = \pi \hbar c \Gamma / (3\lambda)^3$ is the saturation intensity for a two-level atom. The transition strength is $q_{e,g,p} = \frac{|(g|\hat{\mathbf{d}} \cdot \epsilon_p|e)|^2}{\sum_{g'} |(g'|\hat{\mathbf{d}}|e)|^2}$, where $\hat{\mathbf{d}}$ is the dipole moment operator and ϵ_p is the laser polarization. From these definitions, $q_{e,g,p} s_p = 2\Omega_{e,g}^2/\Gamma$, where $\Omega_{e,g}$ is the Rabi frequency at which the e - g transition is driven.

B. Zeeman splitting of $X\ ^2\Sigma^+$ and $A\ ^2\Pi_{1/2}$ states

To demonstrate the real MOT force, we take the full nonlinear Zeeman splitting of the ground states. Figure 1(a) shows the relevant energy levels of the X state up to 20 G used in the equations. As seen, the $X(v=0, N=1)$ state is split

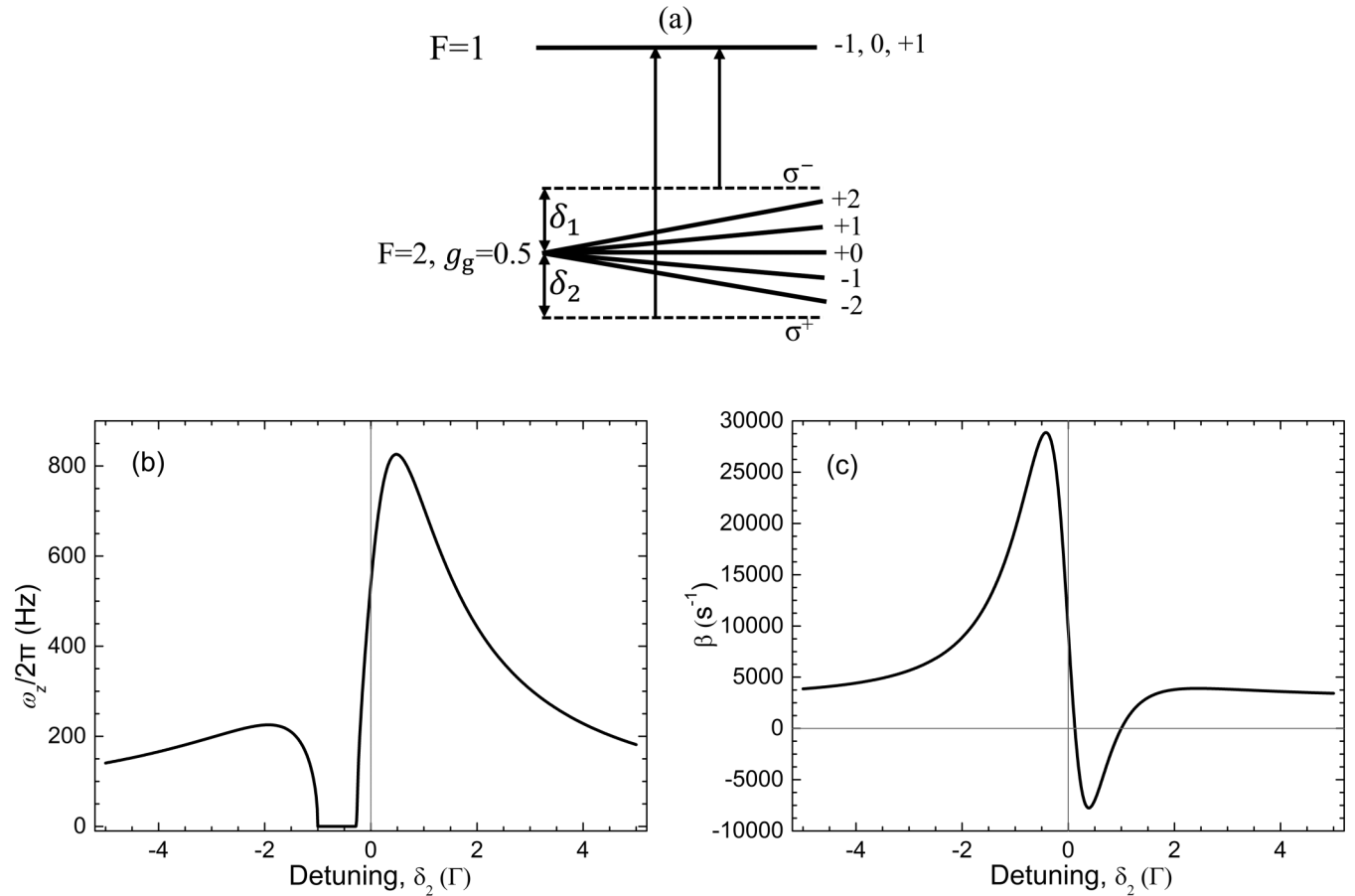


FIG. 2. (a) Illustration of the dual frequency with ground level $F_g = 2$, $g_g = 0.5$ and excited level $F_e = 1$, $g_e = 0$. Two transitions with oppositely polarized frequency components were driven, and the detunings are δ_1 and δ_2 , respectively. (b) Trap frequency vs δ_2 . (c) Damping coefficient vs δ_2 .

into four components due to the spin-rotation and hyperfine interactions, which are $F = 1, 0, 1$, and 2 , respectively. The g factors of the ground states, g_g , are given in parentheses after the F labels in Fig. 1(a). In the MOT modeling, all four components are addressed. For the A ($v = 0, J = 1/2, +$) state, we use linear Zeeman shifts given by their g factors, as shown in parentheses in Fig. 1(b). Note that the $F = 1$ level is made up of three Zeeman sublevels, though it cannot be distinguished because of the much smaller g factor. The interval between the $F = 1$ and $F = 0$ levels was set to 10 MHz since the hyperfine splitting of the A state is unknown and indistinguishable. Within the natural width $\Gamma(2\pi \times 22 \text{ MHz})$ of the $A \ ^2\Pi_{1/2}$ state, the interval has minimal influence on our modeling results.

C. The dual-frequency effect

We also consider the dual-frequency effect in the system in Fig. 2(a). The system consists of a ground level with $F_g = 2$, $g_g = 0.5$, an excited level with $F_e = 1$, $g_e = 0$, and two kinds of oppositely polarized frequency with detuning δ_1 and δ_2 . The wavelength, mass, and decay rate are all set equal to the MgF system. The molecule interacts with six orthogonal laser beams, each of which contains two frequencies. The power of each frequency is set to 40 mW, whose saturation parameter is ~ 0.28 . The δ_1 value is fixed to $-\Gamma$, and the δ_2

value is varied. An effective way to demonstrate the trapping and cooling force of the MOT is to calculate the acceleration of a stationary molecule versus its displacement along the z axis, and the acceleration of a molecule at the center of the MOT versus its speed in the z direction. For small values of the displacement, z , and speed, v_z , we can write the acceleration as $a_z = -\omega_z^2 z - \beta v_z$, where $\omega_z/2\pi$ is the trap frequency and β is the damping coefficient. Both of them can be used to characterize the MOT.

Figure 2(b) shows the trap frequency versus δ_2 . Here, we give a brief description of the results. The restoring force has a maximum at about 0.5Γ and remains significant for large positive detuning. There is no trapping when δ_2 varies from $-\Gamma$ to -0.3Γ . However, there is still a considerable trapping force for $\delta_2 < -\Gamma$. These characteristics are attributed to the Zeeman splitting combined with multifrequency lasers, which are named the dual frequency [25].

Figure 2(c) shows the dependence of the damping coefficient on δ_2 . The cooling effect occurs when β is positive. When $\delta_2 < 0$, it is always cooling. While $0 < \delta_2 < \Gamma$, it is heating instead. When $\delta_2 > \Gamma$, it is cooling again.

III. COOLING AND TRAPPING FORCE IN MOT

Now, we move to the model of MOT for the $A(0) - X(0)$ transition of the MgF molecule. This transition has

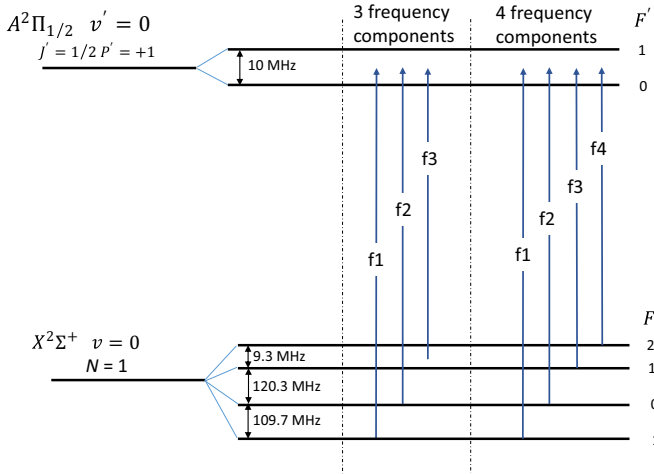


FIG. 3. Schemes for driving the $A(0) - X(0)$ transition in a MOT of MgF. In the three-frequency configuration, f1, f2, and f3 are accordingly relative to the $F = 1$, $F = 0$, and the upper $F = 1, 2$ levels. For the four-frequency case, f1, f2, f3, and f4 are relative to the $F = 1, 0, 1$, and 2 state, respectively.

$\lambda = 359.3$ nm and $\Gamma = 2\pi \times 22$ MHz. The branching ratios of the $A(v = 0, J = 1/2, +) - X(v = 0, N = 1)$ transition were calculated by Yang [30]. Since the interval between the upper $F = 2$ and $F = 1$ is 9.3 MHz, which is less than Gamma (Γ), either three or four frequencies can be used to drive the four hyperfine components of the transition, and the specific structures are shown in Fig. 3. From bottom to top, the intervals between the hyperfine level are, in Γ , 5.0, 5.5, and 0.4, which make the MgF molecule a suitable molecule for the dual frequency. Table I lists the relative frequencies of these components. In our model for the three-frequency configuration, the f1 and f2 frequencies drive the $F = 1$ and $F = 0$ transition, respectively, and the upper $F = 1, 2$ transition is addressed by the f2 and f3 frequencies, which construct the dual-frequency structure. For the four-frequency case, the upper $F = 1, 2$ transition is driven by the f2, f3, and f4 frequencies. For simplicity, there is a global detuning for the three-frequency component model, while for the four-components case we consider two kinds of detuning, which are named δ_1, δ_2 , due to the specific level structure between the $F = 2$ and the upper $F = 1$ states. The f1, f2, and f4 components share the same δ_1 , and the f3 has a separate δ_2 . A more general case with three or four different detunings

TABLE I. From left to right are the energy splitting of the hyperfine structure of $X(0)$ and the frequency of each component in the three- and four-frequency schemes, respectively.

F	$X(0)$ (MHz)	Three-frequency scheme (MHz)	Four-frequency scheme (MHz)
1	-166.4	f1	-166.4
0	-56.6	f2	-56.6
1	63.7	f3	63.7
2	72.9		f4

instead of a global detuning would have little effect on the conclusions of the whole paper.

A. Three-frequency component model

Figure 4 shows the results for the three-frequency case. Both the acceleration of a stationary molecule for a range of positions along the z axis of the MOT and the accelerations for a range of velocities for a molecule at the origin are obtained for various values of detuning and polarizations. If all sets of polarizations are reversed, the position-dependent acceleration changes sign. There are four different configurations for three kinds of laser polarization. We denote the polarization of the frequency components as $(\pm \pm \pm)$, for the case where the f1, f2, f3 components have polarization $\sigma^\pm \sigma^\pm \sigma^\pm$, respectively.

From Figs. 4(a) and 4(b), we can see that the $(+++)$ and $(+--)$ configurations perform worse than the other two cases in restoring and damping force. This can be explained by the same polarization of f2 and f3 since they violate the dual-frequency mechanism. A molecule in dark states, relative to f3, is also not able to be pumped to cycling by f2. The minor differences between $(-+-)$ and $(++-)$ show that the main part of the force is supplied by the $F = 2$ state, that is to say, the dual-frequency effect is the main mechanism responsible for the trapping force when the $A^2\Pi_{1/2} - X^2\Sigma^+$ transition is concerned. Note that although the f2 and f3 components can form a restoring force for the $F = 2$ level, they also generate the antirestoring force for the upper $F = 1$ level. This is the reason that the total trapping force is less than half of that of the four-frequency configuration. In short, for the three-frequency configuration, both $(++-)$ and $(-+-)$ appear to be good choices.

Figures 4(c) and 4(d) show how the acceleration depends on position and speed for various values of detuning. The solid line represents the $(++-)$ configuration while the dashed line is the $(-+-)$ case. For the $(++-)$ scheme, when the detuning is positive, it heats the molecule and pushes the molecule away from the center. While the detuning is smaller than -0.5Γ , there is a net trapping and damping force and the optimum detuning is $-\Gamma$ after considering the two kinds of force comprehensively. On the other hand, the trapping acceleration of the $(-+-)$ case always exists throughout the values of detuning that we investigated and the velocity-dependent acceleration of the $(-+-)$ scheme is almost overlapped with the $(++-)$ one. The optimal detuning for $(-+-)$ is also $-\Gamma$. To find the capture velocity of the MOT, v_c , we consider that molecules enter the MOT in the x - y plane and are at 45° to the laser beams. We calculate the fastest speed a molecule can have if it is to be captured. Though the damping forces vary greatly with the global detuning, they almost pass through the same point with acceleration equal to zero, $v_c = 23$ m/s.

We also investigated the dependence of the MOT force of MgF on the power of each frequency component. Since the saturation intensity of the MgF molecule is 62.5 mW/cm², which is much bigger than that of CaF and SrF, it can withstand greater laser intensity without oversaturation. The

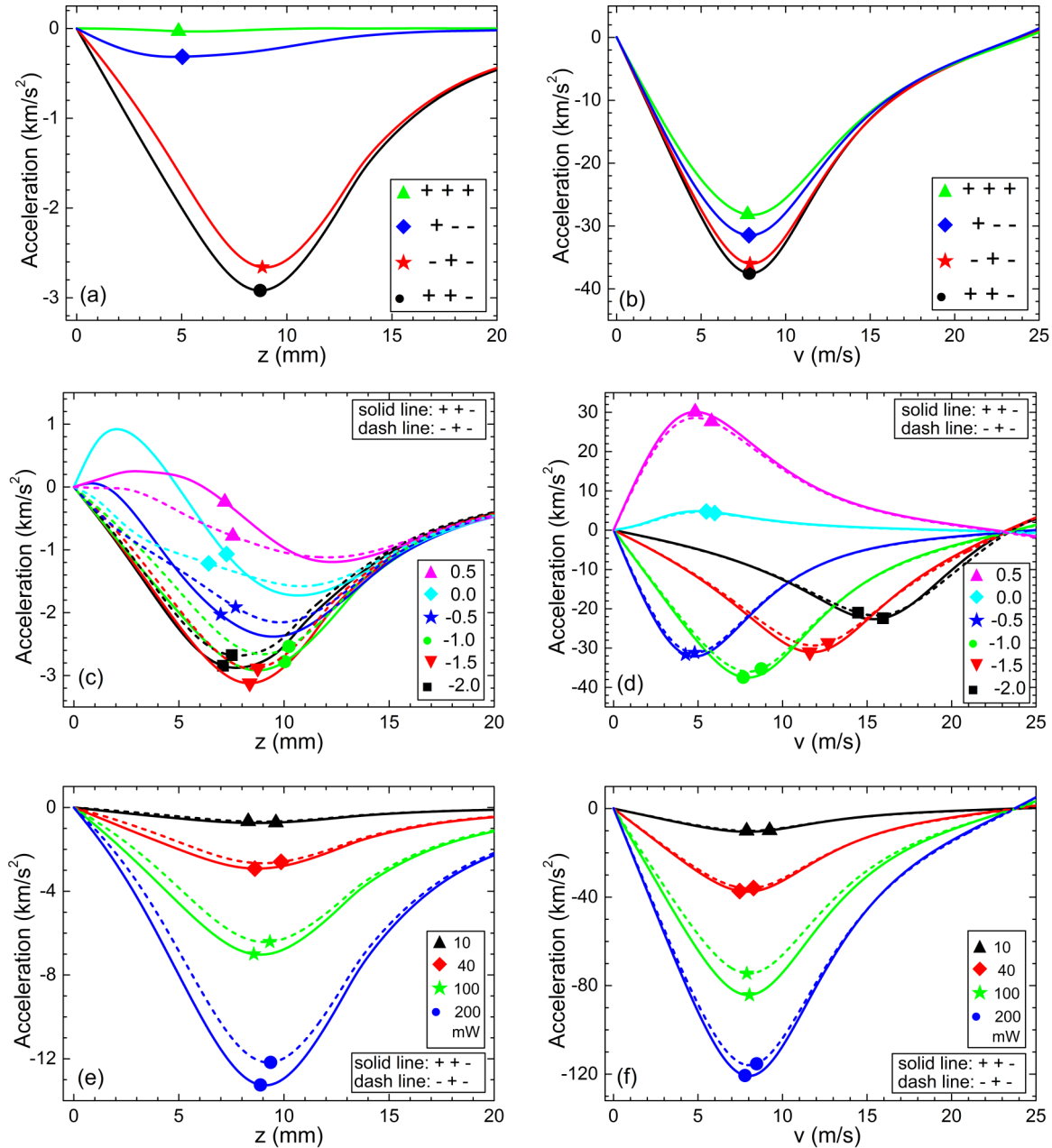


FIG. 4. Acceleration curves vs (a) displacement and (b) speed, where the $A(0) - X(0)$ transition is driven using three-frequency components. The values of the power for f_1 , f_2 , and f_3 are 40, 40, and 80 mW, respectively. The detuning is $-\Gamma$. Acceleration vs (c) displacement and (d) speed, for six different values of the detuning: -2.0 , -1.5 , -1.0 , -0.5 , 0.0 , and 0.5Γ . The solid line represents the $(+ + -)$ configuration, while the dashed line is the $(- + -)$ case. The power of each frequency component is the same as (a). Acceleration vs (e) displacement and (f) speed, for four various values of the power for the f_1 frequency component: 10, 40, 100, and 200 mW, where the power ratio of f_1 , f_2 , and f_3 is 1: 1: 2. The detuning is $-\Gamma$.

saturation parameters at 10, 40, 100, and 200 mW are 0.07, 0.28, 0.7, and 1.4, respectively. We only consider the values of laser power up to 200 mW because the maximum output power of our laser system is ~ 1 W, which will be distributed to the four hyperfine levels. We can see from Figs. 4(e) and 4(f) that both the trapping and damping acceleration continue to increase as the laser power is increased up to 200 mW. We see that the damping force peaks when the speed is near 8 m/s, corresponding to a Doppler shift that is equal to the detuning of $-\Gamma$.

B. Four-frequency component model

The four-frequency case is complicated because there are more combinations and we set two kinds of detuning. To find the optimum polarization and detuning, we calculated the trapping frequency and the damping coefficient versus its detuning δ_1 and δ_2 , for eight different polarization configurations. For simplicity, we only show the results of $(+ + + -)$, which are in Figs. 5(a) and 5(b). When $-1.0\Gamma < \delta_1 < 0$ and $-1.5\Gamma < \delta_2 < 0$, it provides a larger cooling force and, if the detuning is positive, the result

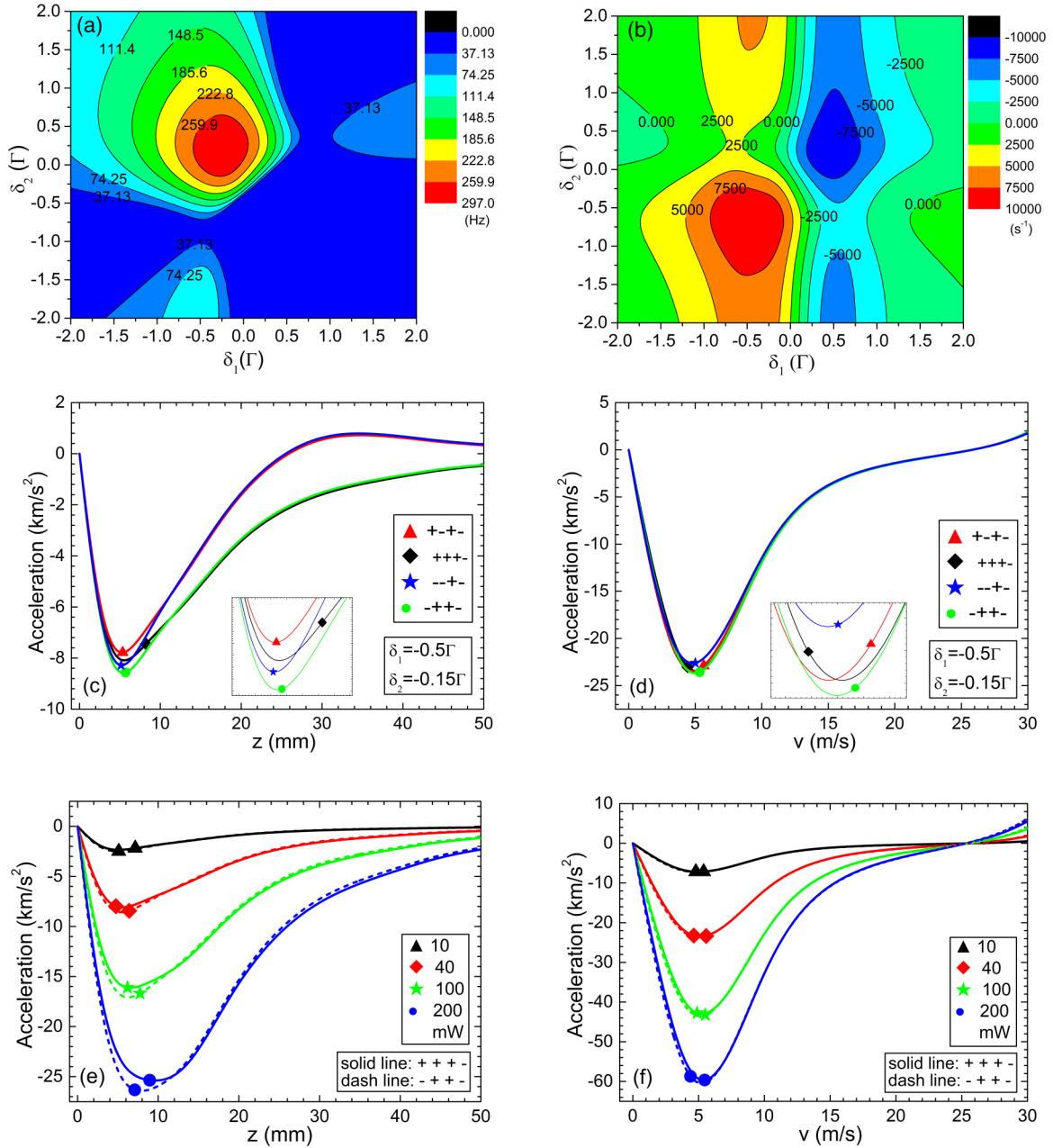


FIG. 5. (a) Trap frequency vs δ_1, δ_2 . (b) Damping coefficient vs δ_1, δ_2 for the $(+++ -)$ configuration. The optimal values of detuning are $\delta_1 = -0.5\Gamma, \delta_2 = -0.15\Gamma$. $P = 40$ mW. Acceleration vs (c) displacement and (d) speed, for four different polarization configurations: $(+ - + -)$, $(+++ -)$, $(- - + -)$, and $(- + + -)$. The detuning is $\delta_1 = -0.5\Gamma, \delta_2 = -0.15\Gamma$ and the power of each frequency component is 40 mW. Acceleration vs (e) displacement and (f) speed, for four various values of the power in each MOT beam and each frequency component: 10, 40, 100, and 200 mW. The solid line represents the $(+++ -)$ configuration, while the dashed line is the $(- + + -)$ case. The detuning is $\delta_1 = -0.5\Gamma, \delta_2 = -0.15\Gamma$.

is almost opposite. For trapping molecules, $-0.75\Gamma < \delta_1 < 0.25\Gamma$ and $-0.25\Gamma < \delta_2 < 1.0\Gamma$ are the optimal ranges. By carefully seeking the overlapping areas, we obtain the optimum detuning: $\delta_1 = -0.5\Gamma, \delta_2 = -0.15\Gamma$. According to the results of our modeling, four kinds of polarization choices can provide relatively large force, which are $(+++ -)$, $(- - + -)$, $(+ - + -)$, and $(- + + -)$, respectively. Then, we calculated the acceleration curves for these four configurations with the optimal detuning, as seen in Figs. 5(c) and 5(d). In general, the damping force is one-third smaller than that

of the three-frequency case, while the trapping force is about one-and-a-half times bigger than that of the three-frequency configuration. The $(+++ -)$ and $(- + + -)$ perform better than that of $(+ - + -)$ and $(- - + -)$ since the trapping acceleration curves of the black rhombus and the green circle are lower than those of the blue pentagon and the red triangle for large displacement, which result in stronger acceleration. The insets in Figs. 5(c) and 5(d) are just for clarity. Also, the difference between the $(+++ -)$ and $(- + + -)$ configurations is too small to be measured by the experiment.

However, for the convenience of experiment, the $(+++-)$ configuration is preferred since the same σ^+ polarization could be addressed by one electro-optic modulator (EOM) at the same time. Similarly, we found the capture velocity is ~ 26 m/s.

Figure 5(e) shows how the acceleration of a molecule depends on the displacement, for the laser power up to 200 mW. We can see that the peaks of the acceleration curve are pushed out from the center of the MOT with the increase of laser power. Figure 5(f) shows how the acceleration depends on speed for various values of power, with detuning fixed to $\delta_1 = -0.5\Gamma$, $\delta_2 = -0.15\Gamma$. We find that the damping force peaks when the speed is near 5 m/s, which is a little bigger than the Doppler shift that equals the detuning of -0.5Γ .

C. More-frequency component model

Based on the above results, the trapping force of the MgF molecule mainly depends on the dual-frequency arrangement of the $F = 2$ state. By carefully selecting laser polarization and detuning, both the trapping and damping force of MgF

MOT are considerable despite the tiny g factor of the A state. It is worthwhile considering whether the force can be further increased by applying the dual-frequency method to several of the hyperfine components. From Fig. 2, we can see that when $\delta_1 = -\Gamma$ and $\delta_2 = 2\Gamma$, both the trapping and damping force are strong. So, we can aim to arrange this situation for the other hyperfine components. Because the $F = 2$ and the upper $F = 1$ components are spaced by 0.4Γ , we cannot have this situation for both of them at the same time. The $F = 0$ state has no Zeeman splitting and no dark state, so there is nothing to be gained from applying the two oppositely polarized frequency components. What remains is the lower $F = 1$ state. Because it has a negative g factor ($g_g = -0.21$), as shown in Fig. 1, we can add one more frequency to address the lower $F = 1$ level for the $(++-)$ configuration, which is detuned by 2Γ from this level and polarized σ^- . As for the $(-+-)$ scheme, the same detuning and the opposite polarization would work. The specific set of three-plus-one frequencies and polarizations are given in the inset of Fig. 6(a), including four Zeeman sublevels of the ground state labeled with a long solid line, the frequency

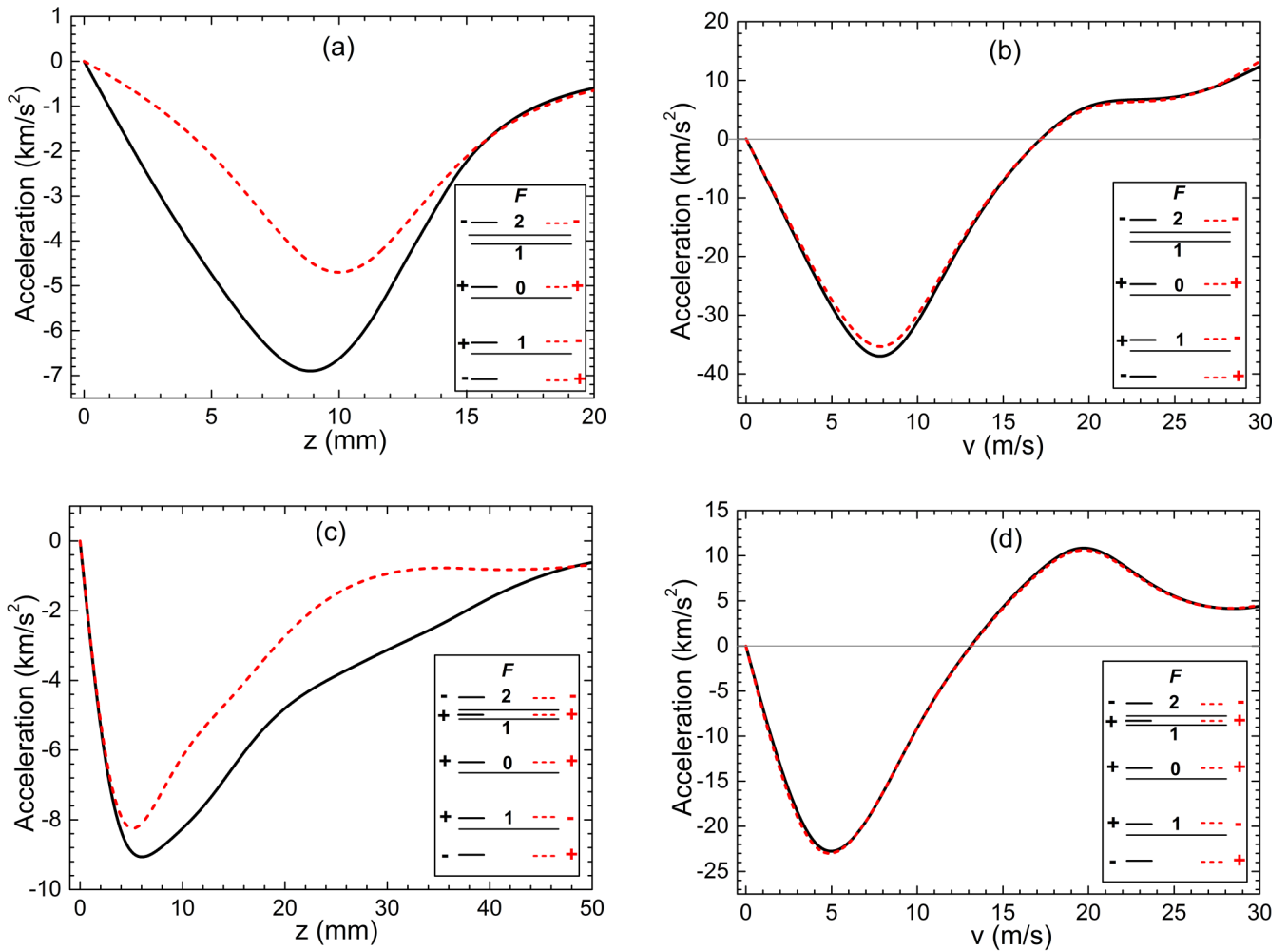


FIG. 6. Acceleration vs (a) displacement and (b) speed, for a MgF MOT operating on the $A(0) - X(0)$ transition using three-plus-one-frequency components. The values of the power for f_1 , f_2 , and f_3 are 40, 40, and 80 mW, respectively. The power of the extra component is 40 mW. The detuning is $-\Gamma$, apart from the additional component whose detuning is 2Γ . Acceleration vs (c) displacement and (d) speed, for a MgF MOT operating on the $A(0) - X(0)$ transition using four-plus-one-frequency components. The detuning is $\delta_1 = -0.5\Gamma$, $\delta_2 = -0.15\Gamma$, and the extra component is detuned by 2Γ . The power of each frequency component is 40 mW.

components of the $(++-)$ configuration labeled with a short solid line, and the frequency components of the $(-+-)$ case labeled with a short dashed line. For the four-frequency component model, a frequency component with polarization σ^- and detuning 2Γ is used to address the lower $F = 1$ state for the $(+++)$ configuration and a frequency component with the same detuning and the opposite polarization is arranged for the $(-+-)$ configuration, giving us the set of four-plus-one frequencies and polarizations illustrated in the inset of Fig. 6(c). Figure 6(a) gives the acceleration versus position for the $(++-)$ and $(-+-)$ configurations. The addition of the extra component more than doubles the maximum acceleration to 7000 m/s^2 for the $(++-)$ case, while the acceleration for the $(-+-)$ scheme is only increased to 4500 m/s^2 . This is because the dual-frequency arrangement of the lower $F = 1$ state—constructed by the extra component—provides an antirestoring force for the $(-+-)$ configuration, though the whole force increases due to the increase of photon scattering. Figure 6(b) shows the acceleration versus speed for the two cases. We find that the additional component has little influence on the maximum damping force or the damping coefficient. But, it slightly narrows down the range of velocities where the molecule can be cooled. The capture velocity decreases to $v_c = 17 \text{ m/s}$. Figure 6(c) illustrated the acceleration versus position for the $(+++)$ and $(-+-)$ configurations. The variations of the trapping force for both $(+++)$ and $(-+-)$ configurations are small. Besides, neither the maximum damping force nor the damping

coefficients change much, as shown in Fig. 6(d). The capture velocity decreases to $v_c = 13 \text{ m/s}$. These results suggest that a three-plus-one-frequency component model, $(-+-)$, is able to provide a relatively large trapping force and the maximum damping force, which means the lowest temperature and the more molecules could be obtained for MgF.

IV. CONCLUSION

We have theoretically modeled the MOT force of MgF with 3D rate equations concerning the dual-frequency mechanism. We discuss some possible options for the polarizations and frequencies of the MOT, and suggest the optimized laser schemes for three-, four-, and more-frequency configurations. Based on the modeling results, a three-plus-one-frequency component scheme is suggested. In short, the MgF molecule is proved to be a good candidate for MOT despite its tiny g factor at the $A^2\Pi_{1/2}$ state.

ACKNOWLEDGMENTS

We acknowledge the financial support from the National Natural Science Foundation of China under Grants No. 11834003, No. 91836103, No. 91536218, and No. 11374100, the Natural Science Foundation of Shanghai Municipality under Grant No. 17ZR1443000, the Joint Research Institute for Science and Society (JoRISS), and the 111 project of China under Grant No. B12024.

-
- [1] E. L. Raab, M. Prentiss, A. Cable, S. Chu, and D. E. Pritchard, *Phys. Rev. Lett.* **59**, 2631 (1987).
 - [2] J. Doyle, B. Friedrich, R. V. Krems, and F. Masnou-Seeuws, *Eur. Phys. J. D* **31**, 149 (2004).
 - [3] D. C. Lincoln, D. David, V. K. Roman, and Y. Jun, *New J. Phys.* **11**, 055049 (2009).
 - [4] D. S. Jin and J. Ye, *Chem. Rev.* **112**, 4801 (2012).
 - [5] K.-K. Ni, S. Ospelkaus, M. H. G. de Miranda, A. Pe'er, B. Neyenhuis, J. J. Zirbel, S. Kotochigova, P. S. Julienne, D. S. Jin, and J. Ye, *Science* **322**, 231 (2008).
 - [6] T. Takekoshi, L. Reichsöllner, A. Schindewolf, J. M. Hutson, C. R. Le Sueur, O. Dulieu, F. Ferlaino, R. Grimm, and H.-C. Nägerl, *Phys. Rev. Lett.* **113**, 205301 (2014).
 - [7] P. K. Molony, P. D. Gregory, Z. Ji, B. Lu, M. P. Köppinger, C. R. Le Sueur, C. L. Blackley, J. M. Hutson, and S. L. Cornish, *Phys. Rev. Lett.* **113**, 255301 (2014).
 - [8] J. W. Park, S. A. Will, and M. W. Zwierlein, *Phys. Rev. Lett.* **114**, 205302 (2015).
 - [9] M. Guo, B. Zhu, B. Lu, X. Ye, F. Wang, R. Vexiau, N. Bouloufa-Maafa, G. Quéméner, O. Dulieu, and D. Wang, *Phys. Rev. Lett.* **116**, 205303 (2016).
 - [10] E. S. Shuman, J. F. Barry, and D. Demille, *Nature (London)* **467**, 820 (2010).
 - [11] E. B. Norrgard, D. J. McCarron, M. H. Steinecker, M. R. Tarbutt, and D. DeMille, *Phys. Rev. Lett.* **116**, 063004 (2016).
 - [12] M. T. Hummon, M. Yeo, B. K. Stuhl, A. L. Collopy, Y. Xia, and J. Ye, *Phys. Rev. Lett.* **110**, 143001 (2013).
 - [13] S. Truppe, H. J. Williams, M. Hambach, L. Caldwell, N. J. Fitch, E. A. Hinds, B. E. Sauer, and M. R. Tarbutt, *Nat. Phys.* **13**, 1173 (2017).
 - [14] L. Anderegg, B. L. Augenbraun, E. Chae, B. Hemmerling, N. R. Hutzler, A. Ravi, A. Collopy, J. Ye, W. Ketterle, and J. M. Doyle, *Phys. Rev. Lett.* **119**, 103201 (2017).
 - [15] I. Kozyryev, L. Baum, K. Matsuda, B. L. Augenbraun, L. Anderegg, A. P. Sedlack, and J. M. Doyle, *Phys. Rev. Lett.* **118**, 173201 (2017).
 - [16] M. Zeppenfeld, B. G. U. Englert, R. Glöckner, A. Prehn, M. Mielenz, C. Sommer, L. D. van Buuren, M. Motsch, and G. Rempe, *Nature (London)* **491**, 570 (2012).
 - [17] A. Prehn, M. Ibrügger, R. Glöckner, G. Rempe, and M. Zeppenfeld, *Phys. Rev. Lett.* **116**, 063005 (2016).
 - [18] J. Lim, J. R. Almond, M. A. Trigatzis, J. A. Devlin, N. J. Fitch, B. E. Sauer, M. R. Tarbutt, and E. A. Hinds, *Phys. Rev. Lett.* **120**, 123201 (2018).
 - [19] W. Bu, T. Chen, G. Lv, and B. Yan, *Phys. Rev. A* **95**, 032701 (2017).
 - [20] P. Aggarwal *et al.* (The NL-eEDM Collaboration), *Eur. Phys. J. D* **72**, 197 (2018).
 - [21] G. Z. Iwata, R. L. McNally, and T. Zelevinsky, *Phys. Rev. A* **96**, 022509 (2017).

- [22] L. W. Cheuk, L. Anderegg, B. L. Augenbraun, Y. Bao, S. Burchesky, W. Ketterle, and J. M. Doyle, *Phys. Rev. Lett.* **121**, 083201 (2018).
- [23] L. Caldwell, J. A. Devlin, H. J. Williams, N. J. Fitch, E. A. Hinds, B. E. Sauer, and M. R. Tarbutt, [arXiv:1812.07926](https://arxiv.org/abs/1812.07926).
- [24] L. Xu, Y. Yin, B. Wei, Y. Xia, and J. Yin, *Phys. Rev. A* **93**, 013408 (2016).
- [25] M. R. Tarbutt and T. C. Steimle, *Phys. Rev. A* **92**, 053401 (2015).
- [26] J. Nakagawa, P. J. Dommelle, T. C. Steimle, and D. O. Harris, *J. Mol. Spectrosc.* **70**, 374 (1978).
- [27] T. C. Steimle, P. J. Dommelle, and D. O. Harris, *J. Mol. Spectrosc.* **73**, 441 (1978).
- [28] M. R. Tarbutt, *New J. Phys.* **17**, 015007 (2015).
- [29] S. Xu, Y. Yin, R. Gu, M. Xia, L. Xu, L. Chen, Y. Xia, and J. Yin, *Rev. Sci. Instrum.* **89**, 046103 (2018).
- [30] X. Yang, C. Li, Y. Yin, S. Xu, X. Li, Y. Xia, and J. Yin, *J. Phys. B* **50**, 015001 (2017).